
Fast Computer Vision based Geometry Estimation

Bachelor Thesis

Authors

Cédric Renda, Manuel Tischhauser

Supervisor

Prof. Dr. Guido M. Schuster

Subject

Image Processing

HSR Hochschule Für Technik Rapperswil

May 21, 2020

Abstract

Introduction

Approach

Conclusion

Contents

Abbreviations	1
1 Introduction	3
2 Theory	5
2.1 Camera Calibration in OpenCV	5
2.1.1 The pinhole camera model	5
2.1.2 The distortion model in OpenCV	7
2.1.3 Reprojection error	10
2.1.4 Error propagation as further quality assessment	10
2.2 Measurement with back-light illumination	11
2.2.1 Light source	11
2.2.2 Light ray distribution	11
2.2.3 Light properties	11
2.2.4 Measurement precision changes	11
2.2.5 Image sensor properties	11
3 Development	13
3.1 Calibration	13
3.1.1 Calibration statistics	13
3.1.2 Numpy-checkerboards	14
3.1.3 Possible cause of errors	15
3.2 Software	19
3.3 Hardware	19
3.3.1 Demonstrator	19
3.3.2 Back-light	20
3.3.3 Computer	20
3.3.4 Camera	20
3.3.5 Production cost	21
4 Results	23
5 Conclusion	25
References	27
List of figures	27

List of tables	29
Statement of Plagiarisms	31
A Partial derivatives of the distortion model	35
B Requirements	37
B.1 Assignment	37
B.2 Requirement Specification	38

Abbreviations

RMS Root Mean Square

Chapter 1

Introduction

Chapter 2

Theory

This chapter takes a closer look at the theory and technology applied in this thesis.

2.1 Camera Calibration in OpenCV

Camera calibration is needed to obtain camera parameters like focal length and center point. Further, it provides a method to correct distortions caused by the imperfect optics according to a certain distortion models. For that, images of a known pattern (usually a checkerboard) have to be taken from different view-points and angles. These points provide the training data which is needed to estimate all the coefficients.

This section describes the theory behind the calibration process in OpenCV. Subsections 2.1.1 and 2.1.2 adapt the parts of the theory and notation from the OpenCV 4.3.0 documentation [1], which is the latest version at the time of writing this thesis.

2.1.1 The pinhole camera model

The functions OpenCV provides to calibrate the camera use the so-called pinhole camera model. This model describes, how a 3D-point specified in world-coordinates (P_w) is transformed to a 3D-point in camera-coordinates (P_c) and then further projected onto the image plane (p). After this step, the point is described as a 2D-point in pixel coordinates. Figure ?? illustrates this setup.

The transition from the world-coordinates to the camera-coordinates can be described as

$$\underbrace{\begin{pmatrix} X_c \\ Y_c \\ Z_c \end{pmatrix}}_{P_c} = \underbrace{\begin{pmatrix} r_{11} & r_{12} & r_{13} \\ r_{21} & r_{22} & r_{23} \\ r_{31} & r_{32} & r_{33} \end{pmatrix}}_R \underbrace{\begin{pmatrix} X_w \\ Y_w \\ Z_w \end{pmatrix}}_{P_w} + \underbrace{\begin{pmatrix} t_x \\ t_y \\ t_z \end{pmatrix}}_t.$$

The vector P_w is first rotated by R and then translated by t . This can be written in one single matrix:

$$\begin{pmatrix} X_c \\ Y_c \\ Z_c \end{pmatrix} = \begin{pmatrix} r_{11} & r_{12} & r_{13} & t_x \\ r_{21} & r_{22} & r_{23} & t_y \\ r_{31} & r_{32} & r_{33} & t_z \end{pmatrix} \begin{pmatrix} X_w \\ Y_w \\ Z_w \\ 1 \end{pmatrix} \Leftrightarrow P_c = (R \mid t) \begin{pmatrix} P_w \\ 1 \end{pmatrix}. \quad (2.1)$$

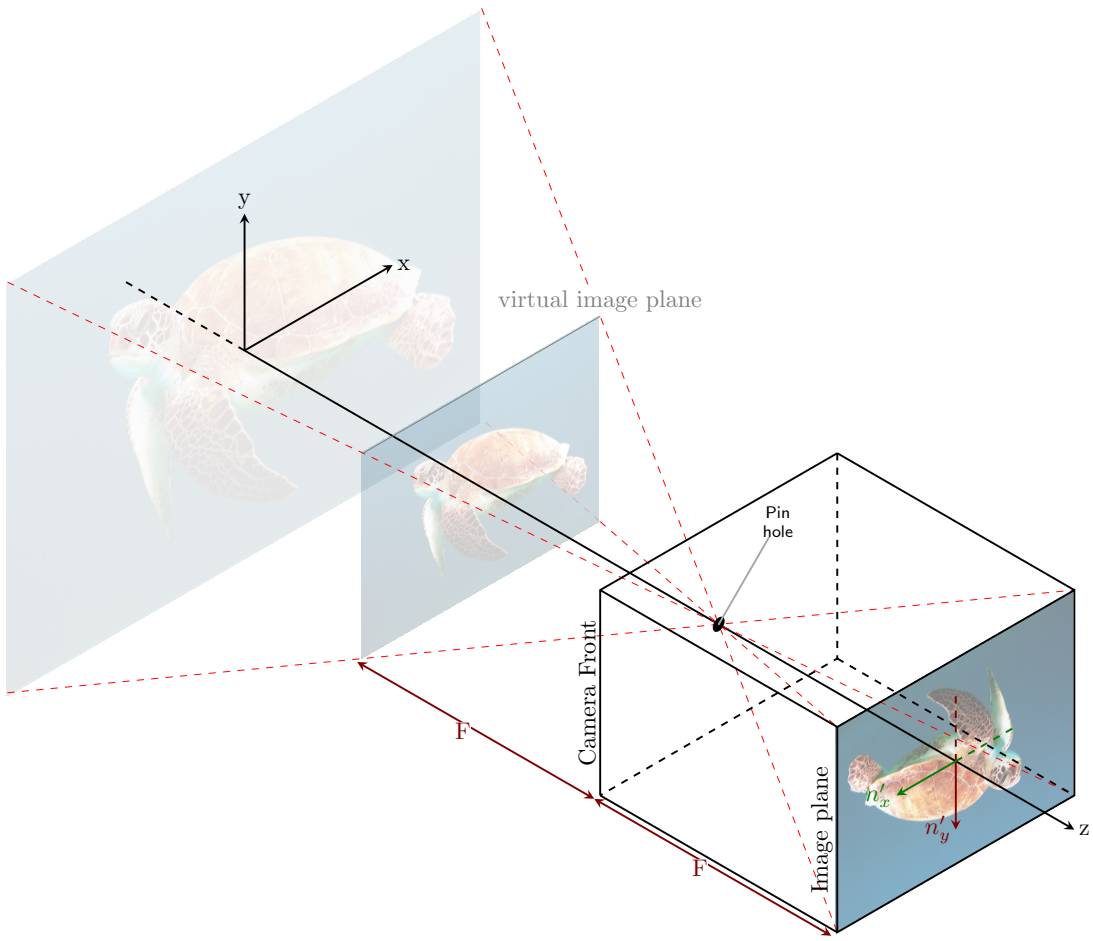


Figure 2.1: Pinhole-model whole camera.

As a result of the theorem of intersecting lines, the projection from P_c to p is described as

$$\underbrace{\begin{pmatrix} u \\ v \\ 1 \end{pmatrix}}_p = \begin{pmatrix} f_x \cdot X_c / Z_c \\ f_y \cdot Y_c / Z_c \\ 1 \end{pmatrix} + \begin{pmatrix} c_x \\ c_y \\ 0 \end{pmatrix}.$$

where f_x and f_y are the focal length f (in world units) normalized by their respective pixel size (in world units). Thus f_x and f_y are the same, if the pixels are quadratic.

By adding the principal point $(c_x \ c_y)^T$, which is usually close to the image center, it is taken into account, that pixel-coordinates are specified with respect to the upper left corner of the image plane. . It is now simpler to write this in homogeneous coordinates:

$$\begin{pmatrix} u \\ v \\ 1 \end{pmatrix} \sim s \begin{pmatrix} u \\ v \\ 1 \end{pmatrix} = \underbrace{\begin{pmatrix} f_x & 0 & c_x \\ 0 & f_y & c_y \\ 0 & 0 & 1 \end{pmatrix}}_K \begin{pmatrix} X_c \\ Y_c \\ Z_c \end{pmatrix} \Leftrightarrow s \begin{pmatrix} p \\ 1 \end{pmatrix} = K \cdot P_c, \quad (2.2)$$

where s is an arbitrary scaling factor and K is called the camera matrix. The overall transition

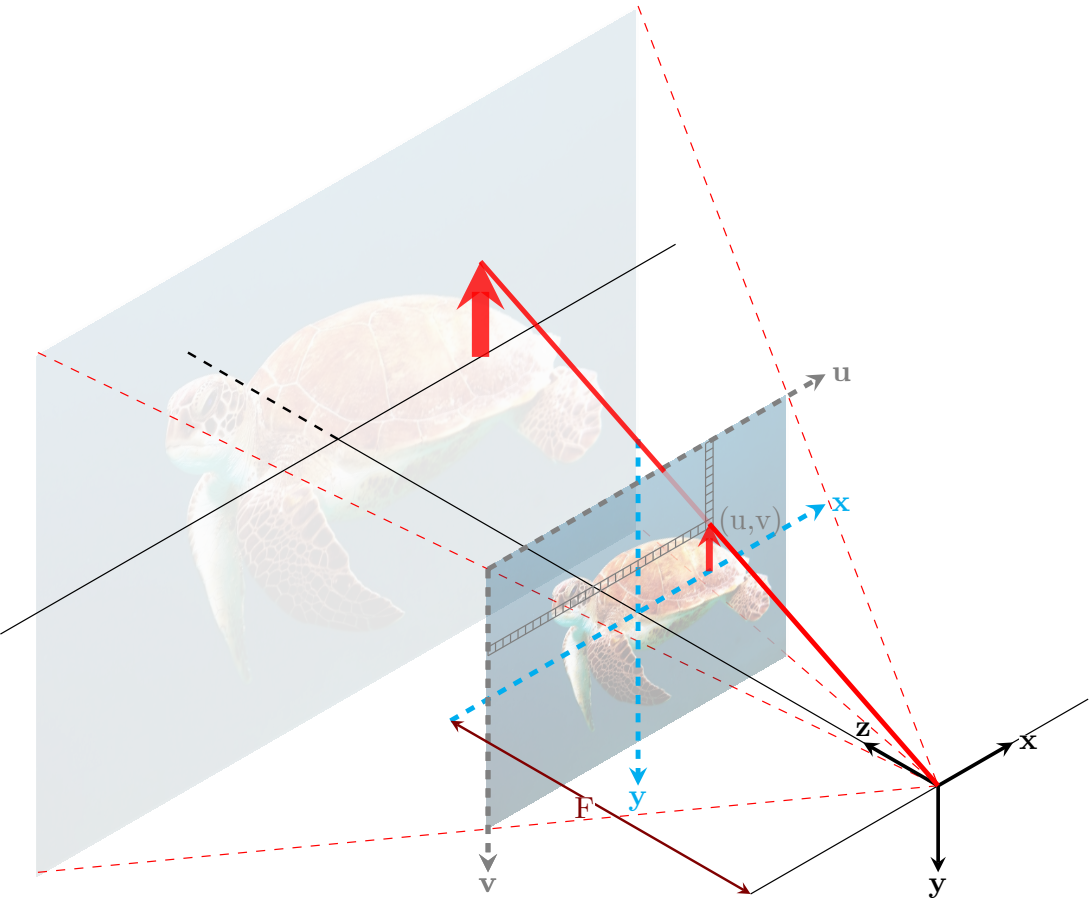


Figure 2.2: Pinhole-model simple model.

from world- to pixel-coordinates is the result of combining 2.1 and 2.2:

$$s \begin{pmatrix} u \\ v \\ 1 \end{pmatrix} = \begin{pmatrix} f_x & 0 & c_x \\ 0 & f_y & c_y \\ 0 & 0 & 1 \end{pmatrix} \begin{pmatrix} r_{11} & r_{12} & r_{13} & t_x \\ r_{21} & r_{22} & r_{23} & t_y \\ r_{31} & r_{32} & r_{33} & t_z \end{pmatrix} \begin{pmatrix} X_w \\ Y_w \\ Z_w \\ 1 \end{pmatrix} \Leftrightarrow s \begin{pmatrix} p \\ 1 \end{pmatrix} = K(R \mid t) \begin{pmatrix} P_w \\ 1 \end{pmatrix} \quad (2.3)$$

The rotation and translation in $(R \mid t)$ are called the extrinsic parameters. The camera matrix K contains analogously the linear intrinsic parameters.

2.1.2 The distortion model in OpenCV

Non linear distortions, which appear before the projection in 2.2 should be considered too. OpenCV takes the effects of radial, tangential and thin prism distortion into account.

Radial Distortion

Radial distortion is caused by the flawed curvature of the lens [2]. It can be modeled with

$$\begin{pmatrix} x'' \\ y'' \end{pmatrix} = \begin{pmatrix} x' \frac{1+k_1r^2+k_2r^4+k_3r^6}{1+k_4r^2+k_5r^4+k_6r^6} \\ y' \frac{1+k_1r^2+k_2r^4+k_3r^6}{1+k_4r^2+k_5r^4+k_6r^6} \end{pmatrix}, \quad (2.4)$$

where x' and y' are coordinates, described in camera-coordinates, normalized with Z_c

$$\begin{pmatrix} x' \\ y' \end{pmatrix} = \begin{pmatrix} X_c/Z_c \\ Y_c/Z_c \end{pmatrix}$$

from and r is the radius as taken with respect to the principal point $(c_x \ c_y)^T$

$$r^2 = x'^2 + y'^2.$$

This type of distortion is symmetrical about the optical axis. Figure 2.3 illustrates the effect on a rectangle.

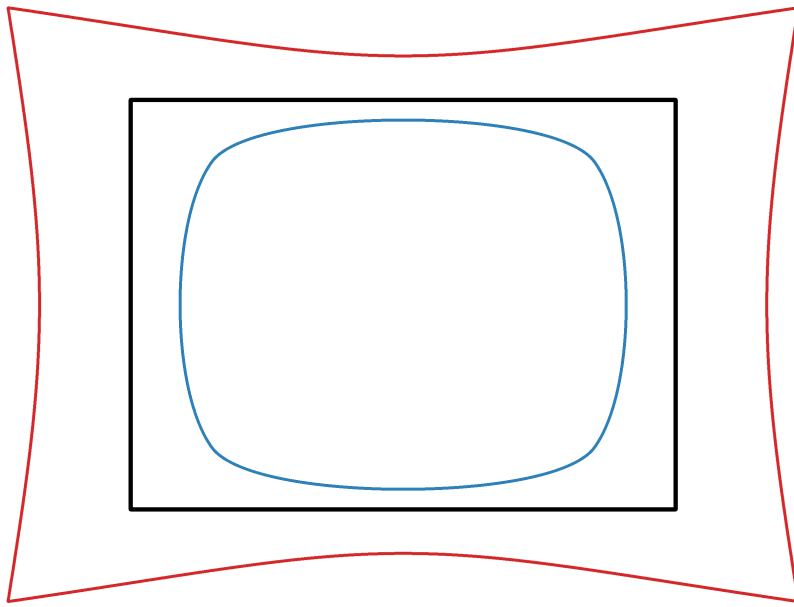


Figure 2.3: Different types of radial distortion. Black: no distortion, red: $k_1 = 10, k_2 = 11, k_3 = 12, k_4 = 5, k_5 = 6, k_6 = 7$, blue: $k_1 = -2.2, k_2 = -1.2, k_3 = -0.8, k_4 = -0.4, k_5 = -0.3, k_6 = -0.2$

Tangential distortion

Real optical systems are also subject to tangential distortion. This type of distortion has a decentering effect and occurs, if the line through the optical center of the lens and the principal point is not col-linear with the optical axis [2]. The model

$$\begin{pmatrix} x'' \\ y'' \end{pmatrix} = \begin{pmatrix} x' + 2p_1x'y' + p_2(r^2 + 2x'^2) \\ y' + 2p_2x'y' + p_1(r^2 + 2y'^2) \end{pmatrix} \quad (2.5)$$

takes this into account. Figure 2.4 shows the distortion this model introduces.

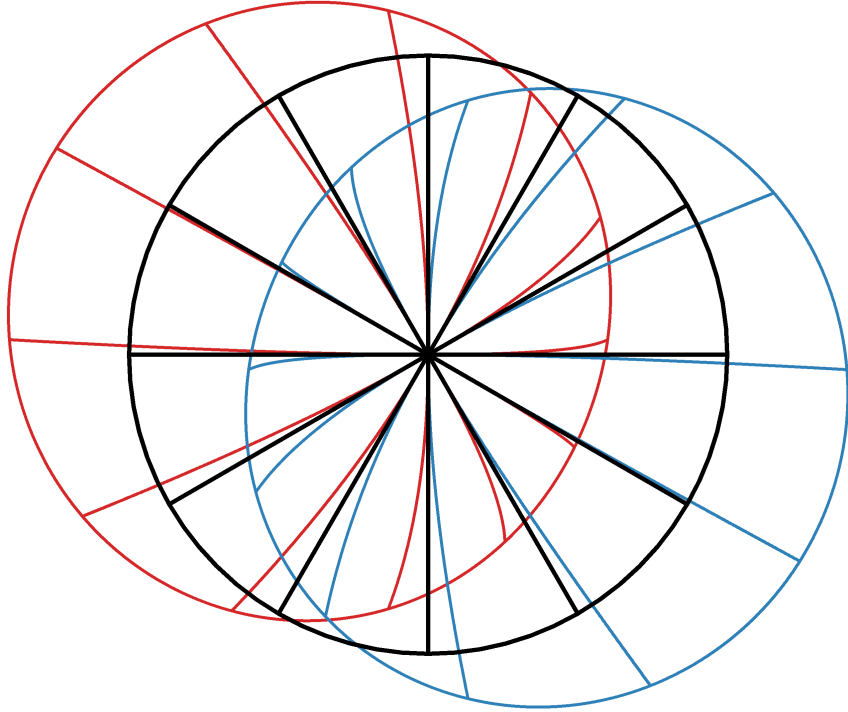


Figure 2.4: Different types of tangential distortion (example adapted from [2]). Black: no distortion, red: $p_1 = -0.15, p_2 = -0.4$, blue: $p_1 = 0.15, p_2 = -0.4$

Thin prism distortion

Thin prism distortion is partially caused by lens imperfections and camera assembly [2]. It introduces additional radial and tangential distortion, modeled with

$$\begin{pmatrix} x'' \\ y'' \end{pmatrix} = \begin{pmatrix} x' + s_1 r^2 + s_2 r^4 \\ y' + s_3 r^2 + s_4 r^4 \end{pmatrix}. \quad (2.6)$$

The combined model in OpenCV

The models in 2.4, 2.5 and 2.6 combined result in

$$\begin{pmatrix} x'' \\ y'' \end{pmatrix} = \begin{pmatrix} x' \frac{1+k_1 r^2 + k_2 r^4 + k_3 r^6}{1+k_4 r^2 + k_5 r^4 + k_6 r^6} + 2p_1 x' y' + p_2(r^2 + 2x'^2) + s_1 r^2 + s_2 r^4 \\ y' \frac{1+k_1 r^2 + k_2 r^4 + k_3 r^6}{1+k_4 r^2 + k_5 r^4 + k_6 r^6} + 2p_2 x' y' + p_1(r^2 + 2y'^2) + s_3 r^2 + s_4 r^4 \end{pmatrix}. \quad (2.7)$$

In summary, a point in normalized camera-coordinates $(x' \ y')^T$ is distorted as modeled in 2.7, which leads to the point $(x'' \ y'')^T$. To get the distorted pixel-coordinates (subscript d), the projection has to be applied

$$\begin{pmatrix} u_d \\ v_d \end{pmatrix} = \begin{pmatrix} x'' f_x + c_x \\ y'' f_y + c_y \end{pmatrix} \Leftrightarrow \begin{pmatrix} u_d \\ v_d \\ 1 \end{pmatrix} = K \begin{pmatrix} x'' \\ y'' \\ 1 \end{pmatrix},$$

which completes the model so far. Keep in mind, that when correcting the distortion, equation 2.7 has to be inverted.

2.1.3 Reprojection error

The reprojection error is a value to asses the quality of a calibration. It is the error between the detected image point and the projection (using the obtained coefficients) of its corresponding world point onto the image plane. Since it only uses the points, which where previously used to obtain the calibration-parameters, it can be interpreted as a training error rate.

Calibration functions in OpenCV return the overall RMS reprojection error [1].

2.1.4 Error propagation as further quality assessment

As argued before, the reprojection error is a training error rate. A low reprojection error is therefore not necessarily enough to estimate, how good the calibration really performs.

OpenCV returns with its extended calibration functions not only the camera intrinsics, but also an estimated standard deviation of each coefficient [1]. Under assumption that low standard deviations suggest a good calibration, it is valid to combine all standard deviations into one value using the propagation of uncertainty.

The propagation of error states that influence of each error of the inputs x_i on the output value y of a function

$$y = f(x_1, x_2, \dots, x_n)$$

can be linearly approximated and summed up to [3]:

$$\Delta y = \sqrt{\sum_{i=1}^n \left(\frac{\partial y}{\partial x_i} \Delta x_i \right)^2}. \quad (2.8)$$

Applied to 2.7, this leads to

$$\Delta x'' = \sqrt{\sum_{i=1}^6 \left(\frac{\partial x''}{\partial k_i} \Delta k_i \right)^2 + \sum_{i=1}^2 \left(\frac{\partial x''}{\partial p_i} \Delta p_i \right)^2 + \sum_{i=1}^4 \left(\frac{\partial x''}{\partial s_i} \Delta s_i \right)^2}$$

and

$$\Delta y'' = \sqrt{\sum_{i=1}^6 \left(\frac{\partial y''}{\partial k_i} \Delta k_i \right)^2 + \sum_{i=1}^2 \left(\frac{\partial y''}{\partial p_i} \Delta p_i \right)^2 + \sum_{i=1}^4 \left(\frac{\partial y''}{\partial s_i} \Delta s_i \right)^2}.$$

It is at this point not intended to go into further computations of the derivatives. If we look at pixel coordinates from the center of the image, respectively $c_x = 0$ and $c_y = 0$, the radius (distance from the centerpoint) can be expressed as

$$r = \sqrt{(f_x \cdot x'')^2 + (f_y \cdot y'')^2}$$

and therefore, if errors in f_x and f_y are neglected, with the propagation in 2.8 applied

$$\Delta r = \sqrt{\left(\frac{\partial r}{\partial x''} \Delta x'' \right)^2 + \left(\frac{\partial r}{\partial y''} \Delta y'' \right)^2}. \quad (2.9)$$

This value Δr can now be plotted over half the diagonal of an image to compare calibration coefficients of different calibration approaches.

2.2 Measurement with back-light illumination

To measure the size and form of an object there are multiple ways. A popular way to get the contour is to place a light source behind the object desired to measure, and aim on the object with an camera. With this method the optical sensors get the silhouette of the object.

2.2.1 Light source

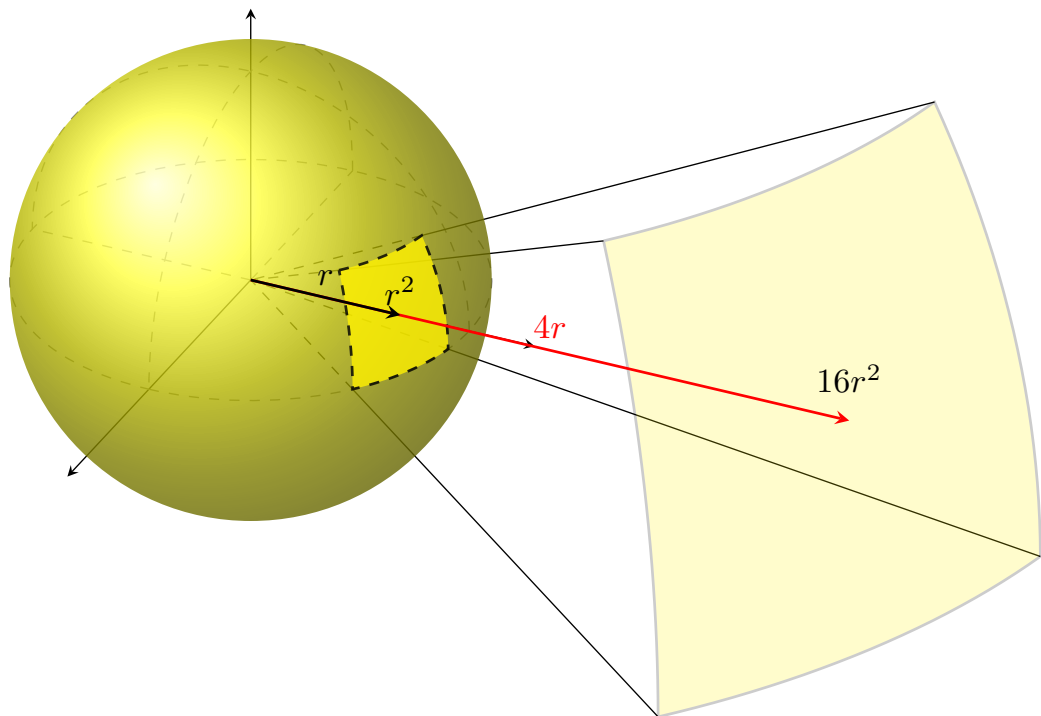


Figure 2.5: Light source in 3d

2.2.2 Light ray distribution

2.2.3 Light properties

2.2.4 Measurement precision changes

2.2.5 Image sensor properties

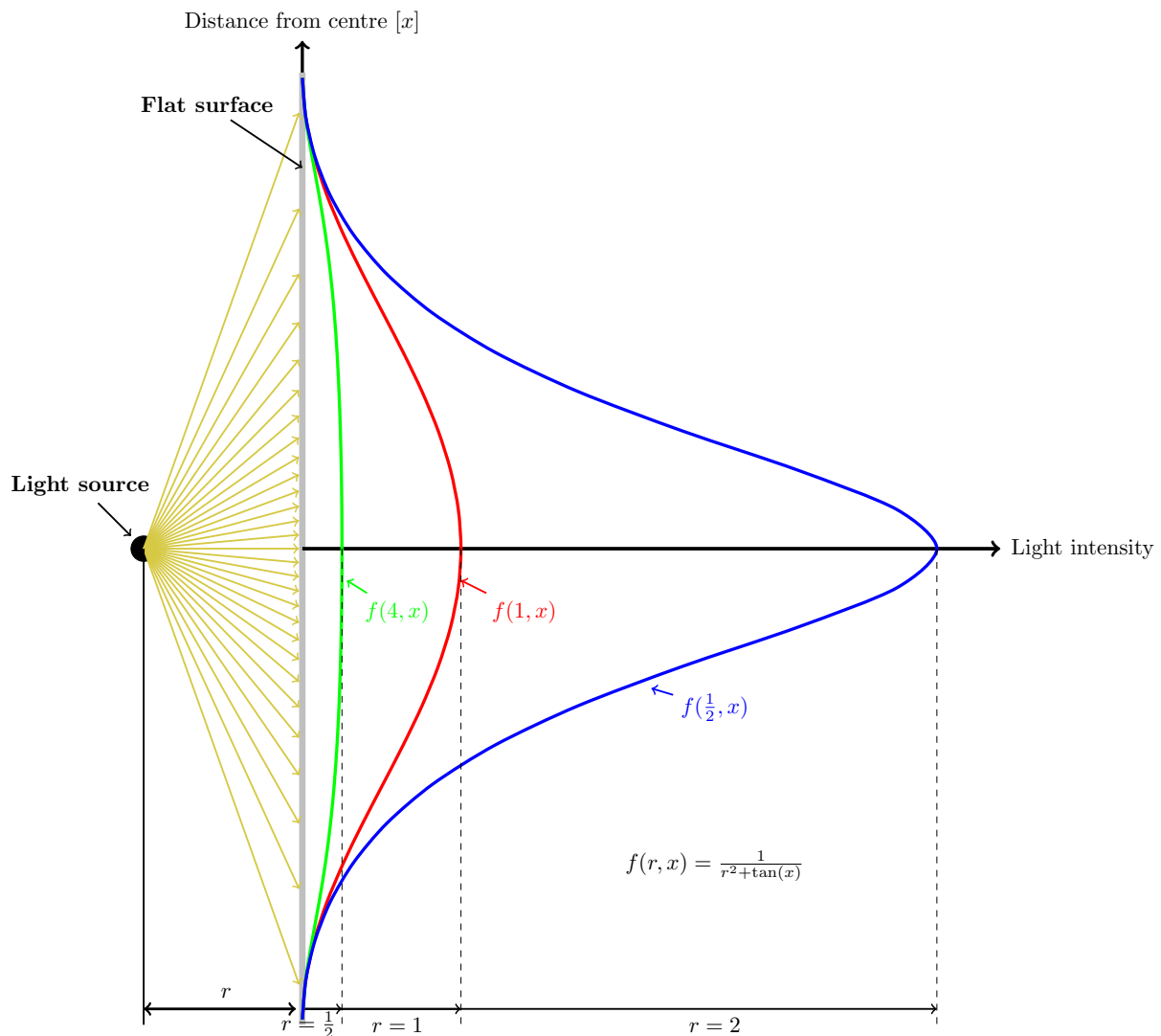


Figure 2.6: Light distribution

Chapter 3

Development

This chapter covers the developing process in more detail.

3.1 Calibration

This section focuses on the calibration of the Raspberry Pi Camera Module V2 (resolution set to 3280×2464 pixels), but all insights learned from these first attempts are applicable to the similar (but higher quality) cameras, which were later also used.

To capture the whole steel-spring, the camera has to be mounted approximately 250 mm away from it. From this distance, one pixel-width corresponds to a length within the tenths of a millimeter range. It is therefore absolutely necessary to calibrate the camera as described in section 2.1, since non-linear distortions can distort the image by 10-20 pixels or even more. Lens imperfections can therefore cause deviations in the measurement of several millimeters, which is not acceptable.

To calibrate a camera in OpenCV, one has to take images of a known 2D-pattern. It is reasonable to use a checkerboard, since OpenCV provides functions to detect checkerboard-corners reliably with subpixel precision.

3.1.1 Calibration statistics

First attempts to calibrate the camera failed. Despite reprojection errors of < 0.3 pixels, the obtained distortion coefficients did not seem to deliver a good undistortion of the image. Furthermore, new attempts with slightly different images of the checkerboard resulted in totally different coefficients. It is therefore important to take a closer look at the technical aspects of the calibration process.

To get more insight what went wrong, some sort of statistics is needed. 200 images of the checkerboard from different view-points and angles have been taken. A couple of these images are shown in Figure 3.1

Randomly selected from these 200 are ten sets of each 20 images. Now, the camera is calibrated separately with each set. To visualize the result, the difference from the (with the model in equation 2.7) distorted and undistorted pixel-position is plotted. And this on all locations of half the diagonal in the upper right quadrant of the image. In other words, we take a look at the distortion between the image center and the upper right corner where the minimal $r_{\min} = 0$, respectively the image center and the maximal radius $r_{\max} = 2051$ which of course depends on the image resolution.

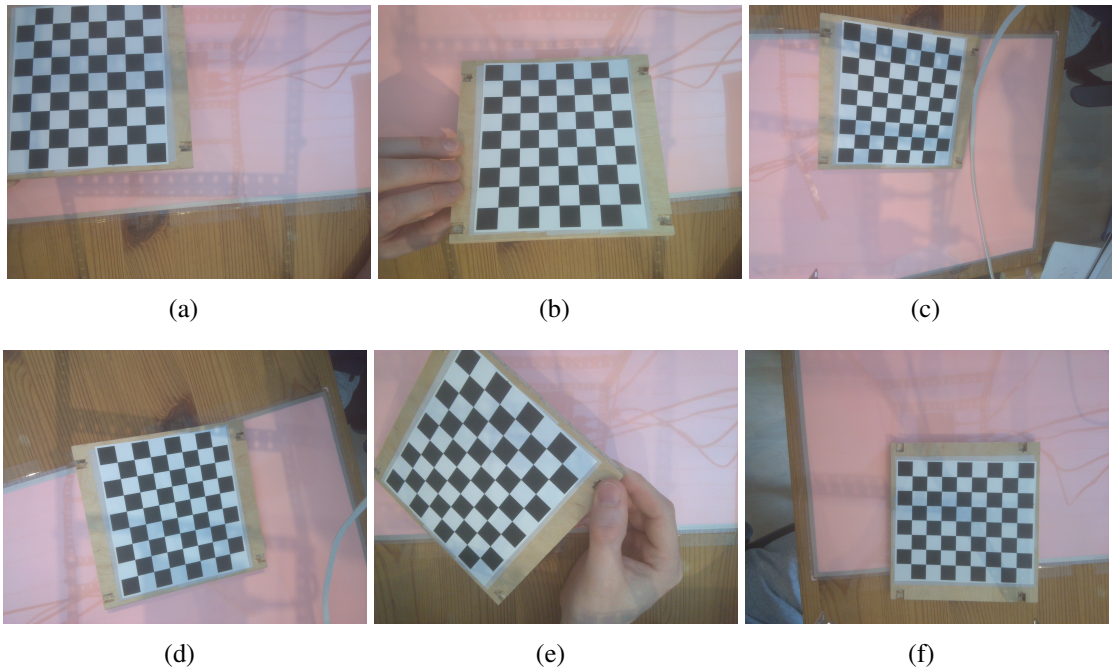


Figure 3.1: Some of the 200 images

This plot is shown in Figure 3.2. Each label displays the reprojection error. The problems which occurred in the first attempts are clearly visible in the scattering of the curves.

The distortion model introduces decentering effects and one could argue, that this plot should be made in all quadrants of the image. But since the decentering effects are rather small in comparison with the radial distortion which is symmetric with respect to the center-point, it should be sufficient to plot only one quadrant. Thus the assumption is made, that if the distortions are high in one quadrant, that the distortions in all other quadrants is also high and vice versa.

3.1.2 Numpy-checkerboards

To estimate the contribution to the bad result of for example additive noise or blurred edges, one has to observe each effect isolated.

In order to do that, a python script was written, which generates a checkerboard as a numpy-array. This array is then translated and rotated in three dimensions, and projected back to the 2D-plane. As a last step, the images are distorted by the model in 2.7 with the coefficients set to:

$$\begin{array}{lll}
 k_1 = 4.1 & k_2 = 36 & k_3 = 38 \\
 k_4 = 4 & k_5 = 34 & k_6 = 40 \\
 p_1 = 0.002 & p_2 = 0.0019 & s_1 = -0.0014 \\
 s_2 = -0.001 & s_3 = -0.0022 & s_4 = 0.00013
 \end{array}$$

These coefficients were not chosen randomly, but were taken from a calibration which was made with one of the ten sets from the calibration statistics in 3.1.1. They should therefore not be completely off. Some of these (in total 24) images are shown in Figure 3.3 To stay close to the real camera, these are not black and white images. The black part has a value of 40 and the white a value of 170. The means of the images come with these values close to 127, which is the value which the exposure control of the camera aims to achieve.

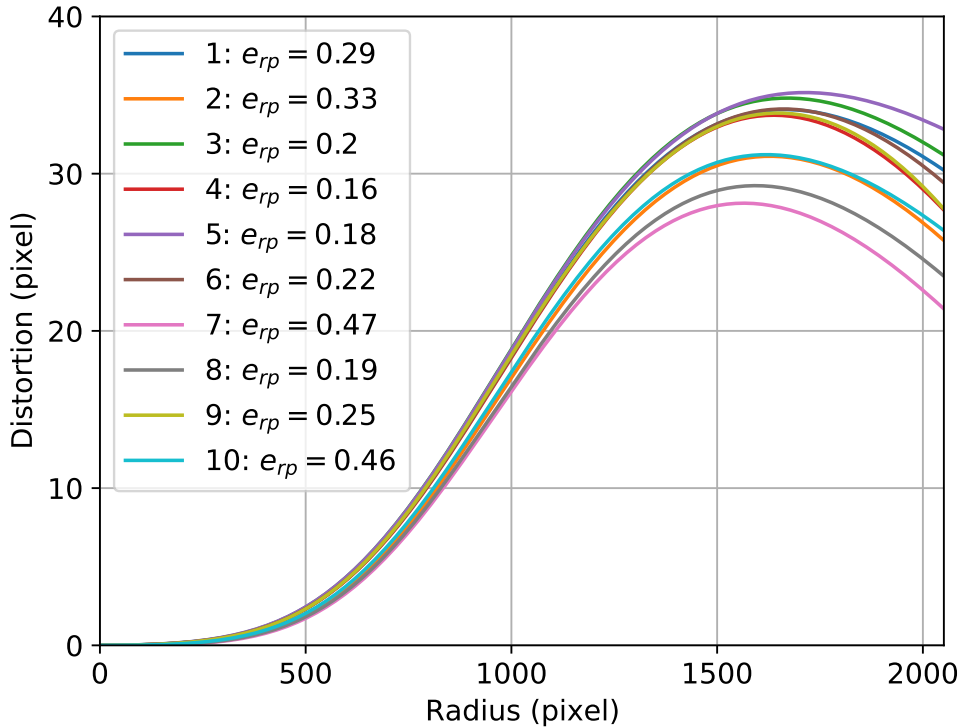


Figure 3.2: Distortion over the radius according to different sets of images

These numpy-checkerboards can now be further manipulated to simulate real effects. To assess how much these effects influence the calibration, the coefficients obtained by the calibration process can be compared to the real coefficients which were used to distort the images in the first place.

3.1.3 Possible cause of errors

This subsection takes a closer look on details, which could be influencing the calibration and lead to the bad results in section 3.1.1. The numpy-checkerboards were hereby used as a basis.

Location of the checkerboard in the image

To show that it is important to include images in the calibration process, in which the checkerboard has corners very close to the image corners, the calibration has been performed two times. The first did include images like 3.3(a) - 3.3(e) and similar, but not images, where the checkerboard reached outside the frame, like 3.3(f). The second calibration included all images.

Again a plot of the distortion, as described in section 3.1.1 is generated. This plot shown in Figure 3.4, contains the real model coefficients and the ones, which were obtained by the calibration. The label displays additionally the reprojection error. There is no discussion that the second calibration (including all images) does a much better job and follows the real curve closer. At the maximal radius, the difference between the model and the second calibration is 2.12 pixel. This also illustrates, that the reprojection error is really a training error rate and is not sufficient to assess the quality of the calibration.

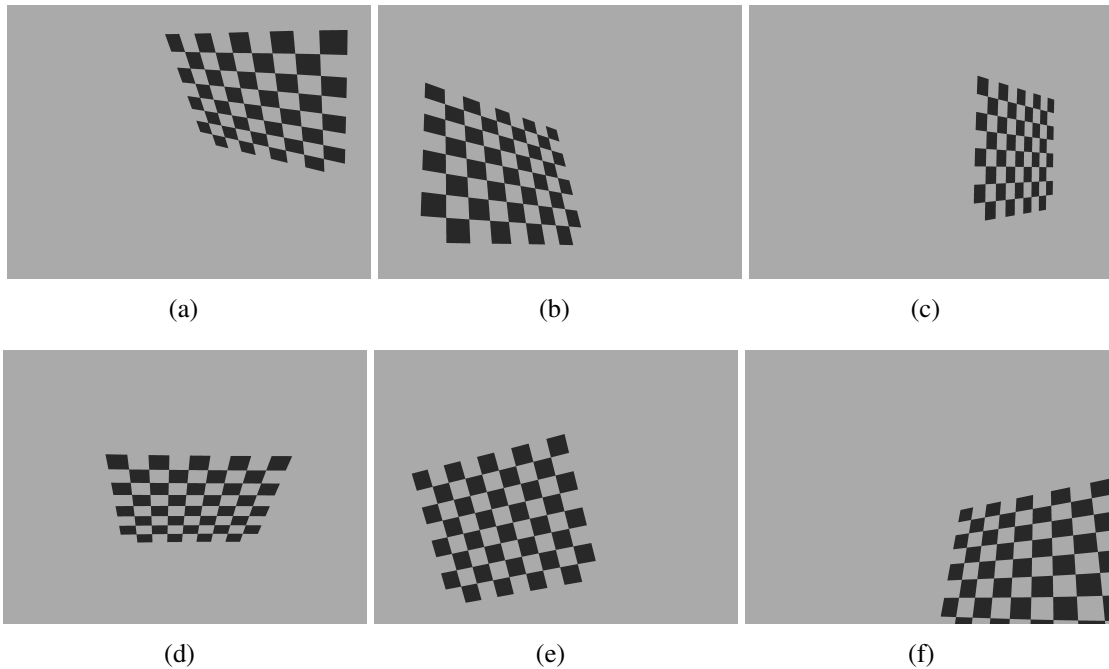


Figure 3.3: Some of the numpy-arrays

One further observation can be made: The second calibration represents some sort of best case calibration. The only error comes from the detection of the checkerboard corners and since these numpy-checkerboards have the sharpest possible edges and there is no noise in the image, it is impossible detect the corners more precise in a real environment with these methods. Thus to get a better calibration, a better feature detection is necessary and its development would take more steps into account which are not in the scope of this thesis.

Additive noise in the image

Exposure in photography contains of three parts: aperture, shutter speed and ISO (light sensitivity). The camera operates in automatic exposure control and tries to fix the average brightness to 127. Since the aperture is fixed, it can only adjust the shutter speed and ISO. If the overall environment is dark, the control needs to make the chip more sensitive against the incoming light by increasing the ISO. This introduces noise into each image.

To get more insight on the properties of the noise, an image of a white background was taken. The histogram of this image with a Gaussian fit is shown in Figure 3.5. Since the background itself is (approximately) uniformly white, there should theoretically only be one spike at the intensity of 127 (fixed by the automatic exposure control). But there is also noise introduced by the chip of the camera, which blurs the histogram. As this plot shows, the assumption that the noise has a normal-distribution is, as one might expect, supported.

To understand now, how much this noise influences the calibration, zero mean additive white Gaussian noise with standard deviations from 0 to 50 (stepsize = 0.5) is added onto each image and the calibration performed.

It turns out, that more noise does not necessarily mean a worse calibration. But there are some insights, which can be taken from this experiment. Figure 3.6 shows how the reprojection error depends on the standard deviation of the additive white noise. It was to be expected, that

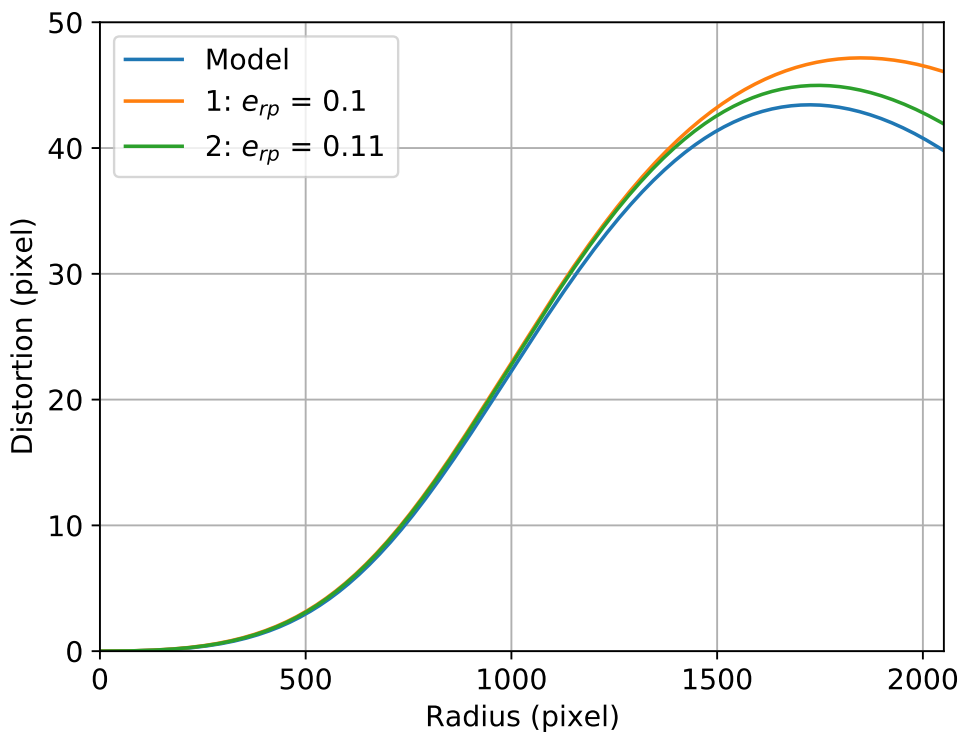


Figure 3.4: Comparison of the calibration to the model. 1: Excluding images with checkerboards overlapping the frame, 2: All images included

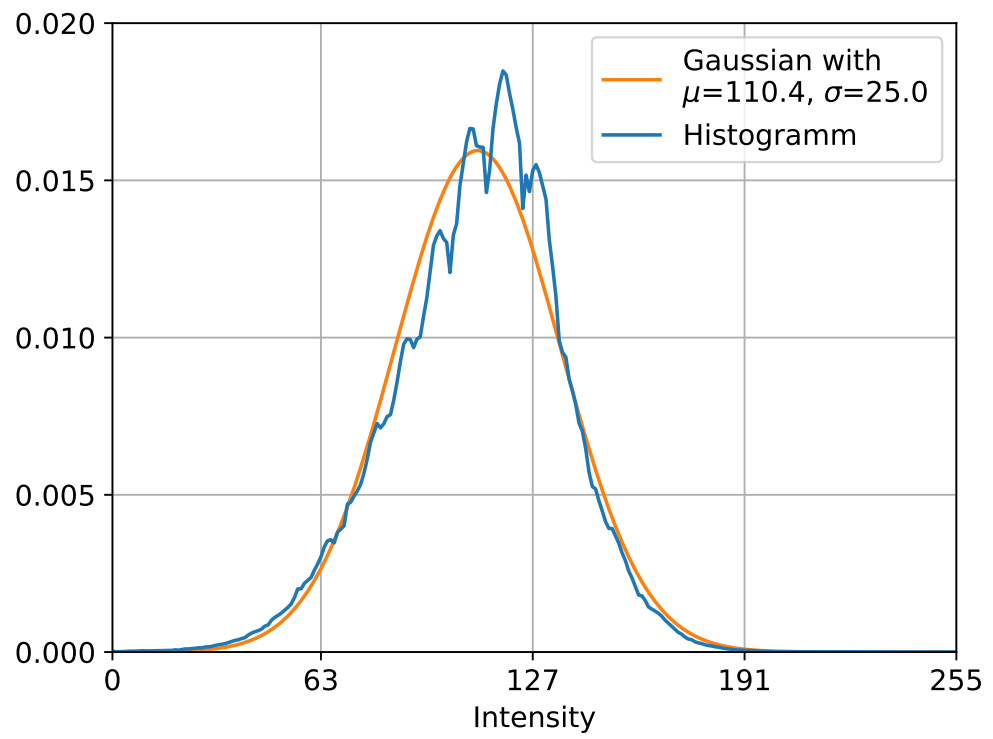


Figure 3.5: Histogram of an uniform white background with an Gaussian fit

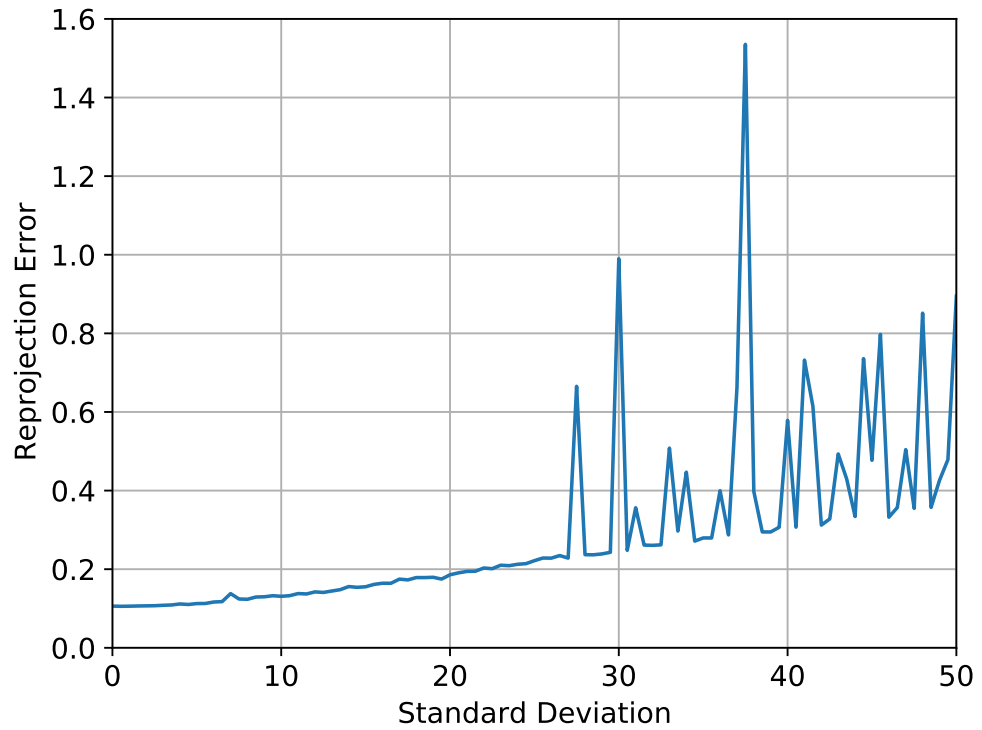


Figure 3.6: Reprojection error in dependence of additive noise

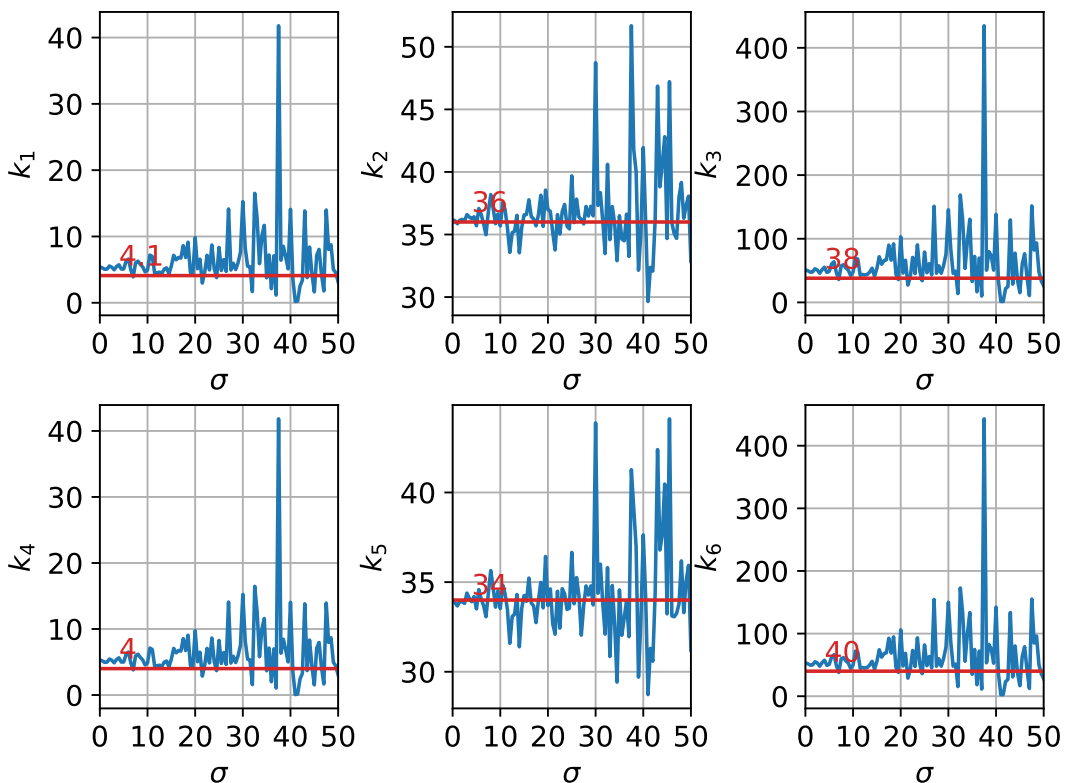


Figure 3.7: Blue: Calibrated radial coefficients in dependence of additive noise (deviation = σ). Red: Real coefficient

the reprojection error increases with more noise, but what really could pose a problem are the spikes. It seems, that after a standard deviation of 25, bad reprojection errors become more likely even if the underlying increase is linear.

This can also be seen in Figure 3.7 where the radial coefficients are plotted. Again it seems that the calibration is not very reliable after a standard deviation of 25. One can conclude, that noise does not affect the calibration directly, but can lead to unreliable results. thus it is necessary to keep noise as low as possible . this can be done by letting enough light reach the camera sensor, that the exposure control can keep the light sensitivity (ISO) low.

Blurred images

To get a grasp how the sharpness of each image affect the calibration, the numpy-checkerboards where convolved with a gaussian kernel of size 61×61 .

3.2 Software

3.3 Hardware

3.3.1 Demonstrator



Figure 3.8: Blurred image

3.3.2 Back-light

The back-light developed for this project had following

3.3.3 Computer

3.3.4 Camera

The camera used for this project had to following evaluation criteria to meet:

- compatible with the Jetson Nano enviroment
- a good developer community
- open source drivers
- low cost
- minimum frame rate of 20[fps]
- measurement accuracy of $\frac{1}{10}$ [mm]

The following is a list of the cameras that have been studied and used in the project:

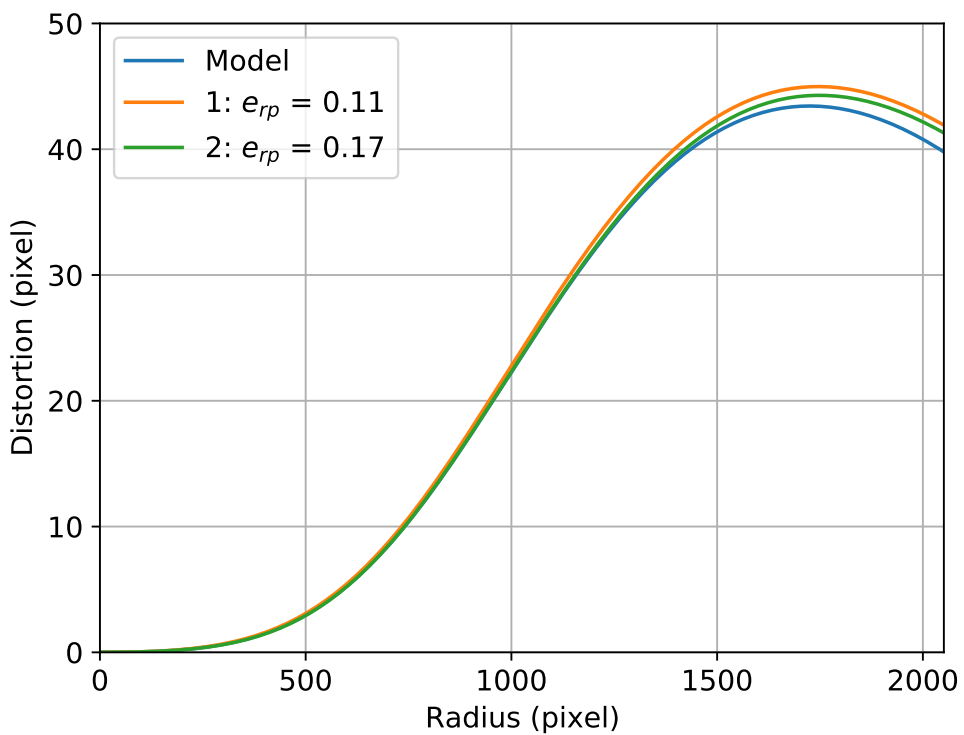


Figure 3.9: Blurred calibration

List of possible Cameras			
Company Camera Name	Raspberry Pi Camera Module V2	Raspberry Pi HQ Camera	Arducam Arducam IMX219 Low Distortion M12 Mount Camera Module
Price	\$25	\$50	\$39.99
Camera Sensor	Sony IMX219	Sony IMX477	Sony IMX219
Still resolution	8M	12M	12.3M
Sensor resolution	3280 x 2464	4056 x 3040	3280 x 2464
Linux integration	V4L2 driver	V4L2 driver	V4L2 driver
Pixel size	1.12 x 1.12 μ m	1.55 x 1.55 μ m	1.12 x 1.12 μ m
Focal length	3.04 [mm]	Depends on lens	2.8 [mm]
Focal ratio	2.0	Depends on lens	2.8
View angle Horizontal	62.2 deg.	Depends on lens	75 deg.

3.3.5 Production cost

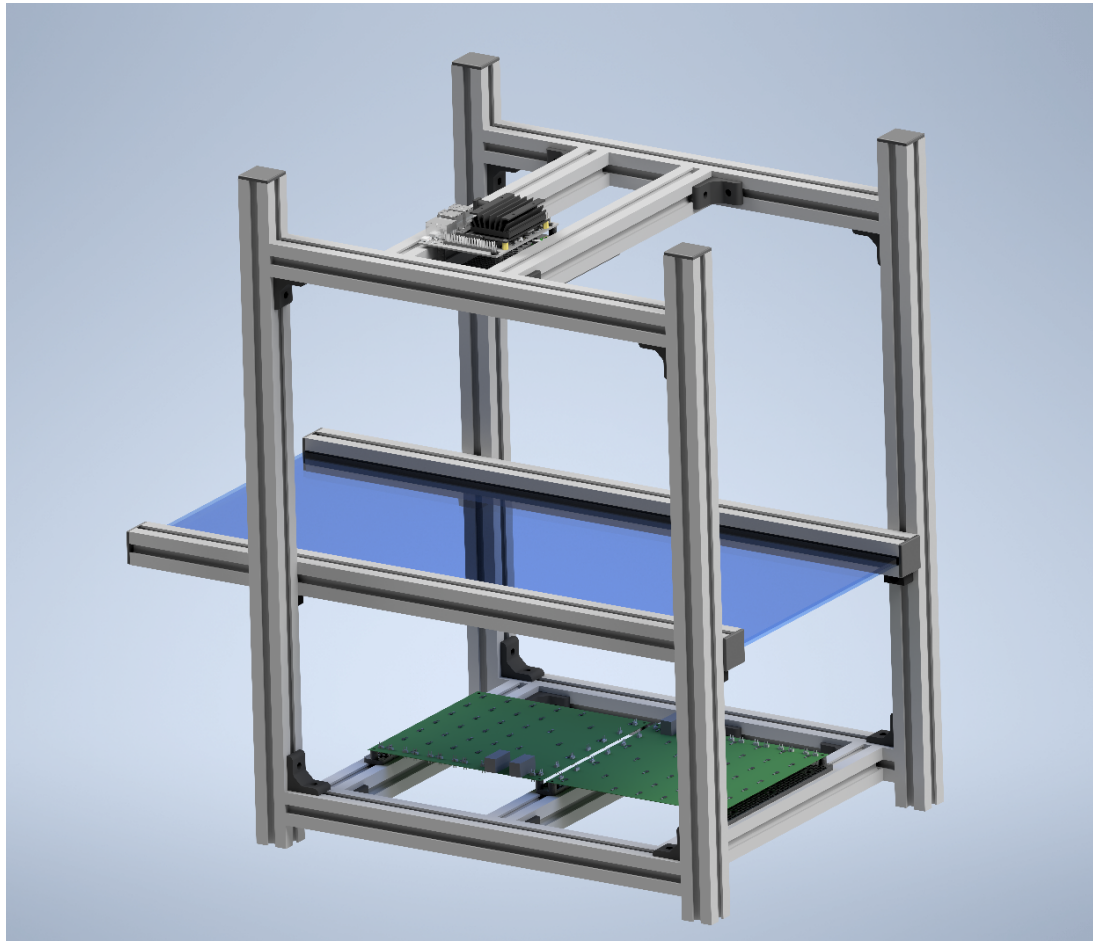


Figure 3.10: 3D-Model of the demonstrator

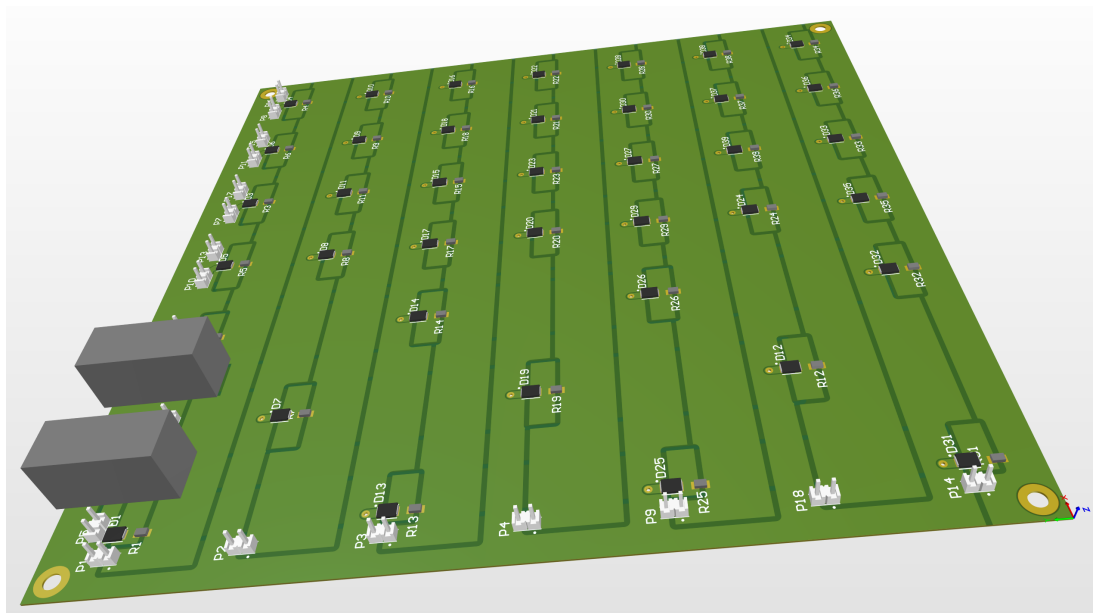


Figure 3.11: 3D-Model of the back-light PCB

Chapter 4

Results

This chapter covers the most important results.

Chapter 5

Conclusion

References

- [1] Bradski, G. (Apr. 2020). Camera Calibration and 3D Reconstruction, [Online]. Available: https://docs.opencv.org/4.3.0/d9/d0c/group__calib3d.html (visited on 05/14/2020).
- [2] J. Weng, P. Cohen, and M. Herniou, “Camera calibration with distortion models and accuracy evaluation,” *IEEE Transactions on Pattern Analysis and Machine Intelligence*, vol. 14, no. 10, pp. 965–980, 1992.
- [3] B. Bucher, “Naturwissenschaftliches praktikum einführung,” Apr. 2017.

List of Figures

2.1	Pinhole-model whole camera.	6
2.2	Pinhole-model simple model.	7
2.3	Different types of radial distortion. Black: no distortion, red: $k_1 = 10, k_2 = 11, k_3 = 12, k_4 = 5, k_5 = 6, k_6 = 7$, blue: $k_1 = -2.2, k_2 = -1.2, k_3 = -0.8, k_4 = -0.4, k_5 = -0.3, k_6 = -0.2$	8
2.4	Different types of tangential distortion (example adapted from [2]). Black: no distortion, red: $p_1 = -0.15, p_2 = -0.4$, blue: $p_1 = 0.15, p_2 = -0.4$	9
2.5	Light source in 3d	11
2.6	Light distribution	12
3.1	Some of the 200 images	14
3.2	Distortion over the radius according to different sets of images	15
3.3	Some of the numpy-arrays	16
3.4	Comparison of the calibration to the model. 1: Excluding images with checkerboards overlapping the frame, 2: All images included	17
3.5	Histogram of an uniform white background with an Gaussian fit	18
3.6	Reprojection error in dependence of additive noise	18
3.7	Blue: Calibrated radial coefficients in dependence of additive noise (deviation = σ). Red: Real coefficient	19
3.8	Blurred image	20
3.9	Blurred calibration	21
3.10	3D-Model of the demonstrator	22
3.11	3D-Model of the back-light PCB	22

List of Tables

Statement of Plagiarism

We declare that, apart from properly referenced quotations, this report is our own work and contains no plagiarism; it has not been submitted previously for any other assessed unit on this or other degree courses.

Place	Date
Rapperswil	May 21, 2020

Signatures

Cedric Renda

Manuel Tischhauser

Appendix A

Partial derivatives of the distortion model

Shown are all partial derivatives of the distortion model in 2.7 which are needed to implement the error propagation in subsection 2.1.4.

$$\begin{aligned}
 \frac{\partial x''}{\partial k_1} &= \frac{r^2 x'}{1 + k_4 r^2 + k_5 r^4 + k_6 r^6} & \frac{\partial x''}{\partial p_1} &= 2x'y' \\
 \frac{\partial x''}{\partial k_2} &= \frac{r^4 x'}{1 + k_4 r^2 + k_5 r^4 + k_6 r^6} & \frac{\partial x''}{\partial p_2} &= r^2 + 2x'^2 \\
 \frac{\partial x''}{\partial k_3} &= \frac{r^6 x'}{1 + k_4 r^2 + k_5 r^4 + k_6 r^6} & \frac{\partial x''}{\partial s_1} &= r^2 \\
 \frac{\partial x''}{\partial k_4} &= -r^2 x' \frac{1 + k_1 r^2 + k_2 r^4 + k_3 r^6}{(1 + k_4 r^2 + k_5 r^4 + k_6 r^6)^2} & \frac{\partial x''}{\partial s_2} &= r^4 \\
 \frac{\partial x''}{\partial k_5} &= -r^4 x' \frac{1 + k_1 r^2 + k_2 r^4 + k_3 r^6}{(1 + k_4 r^2 + k_5 r^4 + k_6 r^6)^2} & \frac{\partial x''}{\partial s_3} &= 0 \\
 \frac{\partial x''}{\partial k_6} &= -r^6 x' \frac{1 + k_1 r^2 + k_2 r^4 + k_3 r^6}{(1 + k_4 r^2 + k_5 r^4 + k_6 r^6)^2} & \frac{\partial x''}{\partial s_4} &= 0
 \end{aligned}$$

$$\begin{aligned}
 \frac{\partial y''}{\partial k_1} &= \frac{r^2 x'}{1 + k_4 r^2 + k_5 r^4 + k_6 r^6} & \frac{\partial y''}{\partial p_1} &= r^2 + 2y'^2 \\
 \frac{\partial y''}{\partial k_2} &= \frac{r^4 x'}{1 + k_4 r^2 + k_5 r^4 + k_6 r^6} & \frac{\partial y''}{\partial p_2} &= 2x'y' \\
 \frac{\partial y''}{\partial k_3} &= \frac{r^6 x'}{1 + k_4 r^2 + k_5 r^4 + k_6 r^6} & \frac{\partial y''}{\partial s_1} &= 0 \\
 \frac{\partial y''}{\partial k_4} &= -r^2 x' \frac{1 + k_1 r^2 + k_2 r^4 + k_3 r^6}{(1 + k_4 r^2 + k_5 r^4 + k_6 r^6)^2} & \frac{\partial y''}{\partial s_2} &= 0 \\
 \frac{\partial y''}{\partial k_5} &= -r^4 x' \frac{1 + k_1 r^2 + k_2 r^4 + k_3 r^6}{(1 + k_4 r^2 + k_5 r^4 + k_6 r^6)^2} & \frac{\partial y''}{\partial s_3} &= r^2 \\
 \frac{\partial y''}{\partial k_6} &= -r^6 x' \frac{1 + k_1 r^2 + k_2 r^4 + k_3 r^6}{(1 + k_4 r^2 + k_5 r^4 + k_6 r^6)^2} & \frac{\partial y''}{\partial s_4} &= r^4
 \end{aligned}$$

Appendix B

Requirements

B.1 Assignment

B.2 Requirement Specification

